Evaluating Mesquite Distribution Using Unpiloted Aerial Vehicles and Satellite Imagery☆

Authors: Page, Michael T., Perotto-Baldivieso, Humberto L., Ortega-S, J. Alfonso, Tanner, Evan P., Angerer, Jay P., et al.

Source: Rangeland Ecology and Management, 83(1) : 91-101

Published By: Society for Range Management

URL: https://doi.org/10.1016/j.rama.2022.03.007

Rangeland Ecology & Management 83 (2022) 91–101

Contents lists available at ScienceDirect

Rangeland Ecology & Management

journal homepage: www.elsevier.com/locate/rama

Original Research

Evaluating Mesquite Distribution Using Unpiloted Aerial Vehicles and Satellite Imagery ☆

Michael T. Page [1], Humberto L. Perotto-Baldivieso [2,*], J. Alfonso Ortega-S [3], Evan P. Tanner [4], Jay P. Angerer [5,#], Rider C. Combs [1], Annalysa M. Camacho [1], Melaine Ramirez [6], Victoria Cavazos [6], Hunter Carroll [6], Kiri Baca [7], Dwain Daniels [8], Tony Kimmet [9]

[1] Graduate Research Assistant, Caesar Kleberg Wildlife Research Institute, Texas A&M University, Kingsville, TX 78363, USA
[2] Associate Professor and Research Scientist, Caesar Kleberg Wildlife Research Institute, Texas A&M University, Kingsville, TX 78363, USA
[3] Professor and Research Scientist, Caesar Kleberg Wildlife Research Institute, Texas A&M University, Kingsville, TX 78363, USA
[4] Assistant Professor and Meadows Endowed Chair of Semi-arid Land Ecology, Caesar Kleberg Wildlife Research Institute, Texas A&M University, Kingsville, TX 78363, USA
[5] Texas A&M AgriLife Research, Temple, TX 76502, USA
[6] Undergraduate Research Technician, Caesar Kleberg Wildlife Research Institute, Texas A&M University, Kingsville, TX 78363, USA
[7] Undergraduate Research Technician, New Mexico State University, Las Cruces, NM 88001, USA
[8] Soil Conservationist, GIS Specialist, USDA-NRCS CNTSC, Fort Worth, TX 76115, USA
[9] National Imagery Leader, GIS Analyst, USDA-NRCS NGCE, Fort Worth, TX 76115, USA

ARTICLE INFO

Article history:
Received 19 March 2021
Revised 17 March 2022
Accepted 21 March 2022

Keywords:
Mesquite height
Point cloud data
Random forests
Sentinel-2
Vertical measurement tool

ABSTRACT

Encroachment of woody plant species on rangelands is of critical concern for rangeland health and function. Recent advances in unpiloted aerial vehicles (UAVs) technology have opened new opportunities for natural resource personnel to quantify features within the landscape. Our goal was to combine information derived from UAV and Sentinel-2 imagery to quantify the presence and spatial distribution of mesquite *(Prosopis glandulosa).* The specific objectives were to 1) evaluate the accuracy of UAVs to estimate mesquite height and 2) classify mesquite using a combination of height metrics and spectral information by combining UAV and Sentinel-2 remote sensing data. We conducted our study in three different ecoregions in Texas. We collected on-site tree height field measurements and created two UAV-derived height outputs at 50 m and 100 m above ground level (AGL). We then used a random forest classification with data derived from the UAV to inform Sentinel-2 imagery of mesquite locations to assess its presence at the landscape level. Linear regression analysis showed that 50-m AGL mesquite height estimates from UAV explained 95% of the variability. Variability explained from 100 m AGL height estimates was slightly lower at 92%. Accuracy assessments from using UAV training data to predict mesquite presence using Sentinel-2 imagery yielded overall accuracy of > 80% for all sites, user accuracies up to 86%, and producer accuracies up to 92%. UAV-derived heights of mesquite were reliable. UAV imagery can be used as training data for Sentinel-2 satellite imagery to assess mesquite presence on Texas rangelands. Being able to combine the high spatial resolution of the UAV imagery with the high temporal resolution of the Sentinel-2 satellite imagery could improve our ability to use UAVs to monitor rangelands.

☆ This research was supported by USDA Natural Resources Conservation Service Agreement (grant NR183A750015C017) and The Rotary Club of Corpus Christi Harvey Weil Sportsman Conservationist Award. The Rene Barrientos Graduate Scholarship fund was provided to M. T. Page, R. C. Combs, and A. M. Camacho. A. M. Camacho is funded by NSF-CREST grant 2019-38422-25543. Monetary support was provided by the Meadows Endowed Professorship to E. P. Tanner. This is manuscript 21-106 from the Caesar Kleberg Wildlife Research Institute at Texas A&M University–Kingsville.

* Correspondence: Humberto L. Perotto-Baldivieso, Caesar Kleberg Wildlife Research Institute, Texas A&M University, Kingsville, TX 78363.
E-mail address: humberto.perotto@tamuk.edu (H.L. Perotto-Baldivieso).
Current address: Jay P. Angerer, USDA Agricultural Research Service, Fort Keogh Livestock and Range Research Laboratory, Miles City, MT 59301, USA.

https://doi.org/10.1016/j.rama.2022.03.007

Introduction

Encroachment of woody plant species on rangelands is of critical concern for rangeland health and function (Ansley et al., 2001; Carey et al., 2012; Shackelford et al., 2013). Woody plant encroachment often occurs with livestock overgrazing, fire suppression, and/or mechanical disturbance (Archer and Stokes 2000; Archer 2010; Ku et al., 2012; Adam et al., 2017; Teleki et al., 2019). Woody plant encroachment can negatively affect ecosystem services by altering soil nutrient cycling, hydrologic cycling, and reduction in herbaceous growth (Schlesinger et al., 2000; Archer et al., 2001; Heaton et al., 2003; Huxman et al., 2005; Wilcox 2007; Mirik and Ansley 2012). The increase of woody plant encroachment has been shown to facilitate decreases in biodiversity because of other species being outcompeted for resources (Ratajczak et al., 2012; Teleki et al., 2019).

Honey mesquite (*Prosopis glandulosa;* hereafter "mesquite") is one of the most invasive native woody species within the southwestern United States (Dahl 1982; Ansley et al., 2001, 2018; Ku et al., 2012; Adam et al., 2017). Its native range expands from northern Mexico and throughout the southwestern United States in 11 states including California, Arizona, New Mexico, Texas, and Louisiana (Ansley et al., 1997; NRCS 2020). The encroachment of mesquite has resulted in loss of native rangelands across the southwest with negative effects on ecosystem functions such as reductions in water yield (Ansley et al., 1997; Ball and Taylor 2003; Nie et al., 2012). Although mesquite has been a part of the Texas landscape since before European settlements, it has become problematic to many ranchers and landowners within its range, which has been attributed to its adaptability and rate of spread into areas where it was not prevalent beforehand (Hennessy et al., 1983; Ansley et al., 1997; Anderson and Roderick, 2003). Mohamed et al., (2011) showed that even under proper grazing management, mesquite encroachment causes adverse effects on perennial grass production, which decreases available forage for livestock production. Because of mesquite's ability to reestablish and spread throughout the landscape, it is essential for rangeland managers to be able to monitor mesquite presence at the landscape level (Adam et al., 2017; Ansley et al., 2018) over time and space. Remote sensing approaches can be a viable solution to monitor mesquite presence across landscapes.

Remote sensing has been used to map and quantify the distribution of mesquite (Musick 1984; Fang et al., 2005; Yilmaz et al., 2008, Mirik and Ansley 2012; Adam et al., 2017). Methods used for monitoring mesquite include Light Detection and Ranging (LiDAR) (Ku et al., 2012), aerial imagery (Ansley et al., 2001), and satellite imagery at multiple resolutions (2–60 m) (Musick 1984; Mohamed et al., 2011; Adam et al., 2017). Ku et al., (2012) were able to use terrestrial LiDAR to estimate mesquite biomass at the plot level (5×20 m). However, LiDAR still remains a costly operation (Iglhaut et al., 2019; Jiang et al., 2020). Ansley et al., (2001) were able to successfully assess increases in mesquite canopy cover from 1976 to 1995 using low-altitude aerial images with high-resolution aerial photography (0.1 m) from a traditional piloted aircraft in North Texas but were limited by temporal flight availability and cost. The use of Digital Orthophoto Quadrangle (DOQQ) imagery from the National Aerial Imagery Program (NAIP) is limited to a revisit time of 2 yr, and spatial and spectral resolution can make species differentiation difficult to achieve when multiple woody species are present. The use of LANDSAT satellite imagery for detecting mesquite species has proven to be effective because of the high temporal resolution (revisit times every 16 d), but its use can be restricted because of the coarse spatial resolution (30 m) and the amount of cloud cover present when data are collected by satellites (Musick 1984; Fang et al., 2005; Yilmaz et al., 2008). These methods have proven to be successful at monitoring mesquite; however, low spatial resolution, high costs for high-resolution imagery, and/or low revisit times may limit continuous monitoring of mesquite (Ansley et al., 2001; Yilmaz et al., 2008; Cunliffe et al., 2016; Gillan et al., 2019). Recent developments of remote sensing platforms such as PlanetScope imagery (Dos Reis et al., 2020) and Sentinel-2 (Drusch et al., 2010) with a higher spatial resolution (3 m and 10–60 m, respectively), spectral resolution (4 and 13 bands, respectively), and revisit times (1–5 d) than LANDSAT (spatial resolution: 30 m; spectral resolution 9 bands; revisit time: 16 d) offer new opportunities to improve the detection, classification, and monitoring of temporal trends of invasive species such as mesquite.

The Sentinel-2 satellite mission from the European Space Agency provides open-access imagery with 13 spectral bands every 5 d (ESA 2021). This data source has grown in popularity in research since its launch in 2015 because of increased spatial and spectral resolutions (e.g., Puliti et al., 2018; Kattenborn et al., 2019; Jensen et al., 2020). Sentinel-2 imagery has been used for vegetation mapping (Addabbo et al., 2016), invasive species monitoring (Jensen et al., 2020), and woody cover spatial distribution (Ng et al., 2017; Kattenborn et al., 2019). Given this higher spatial and spectral resolution, Sentinel-2 has the potential to detect mesquite trees that were not detectable with LANDSAT imagery. However, Sentinel-2 imagery is still too coarse to differentiate small trees (< 1 m^2 cover) in the landscape, which can result in reduced accuracy (Kattenborn et al., 2019; Daryaei et al., 2020). Within the past decade, unpiloted aerial vehicles (UAVs) have become more widely used to assess the volume, amount, and spatial distribution of woody vegetation (Laliberte and Rango 2011; Mayr et al., 2018; Jackson et al., 2020). UAVs may offer opportunities to bridge the gap between satellite imagery and field data collection.

Unpiloted aerial vehicles and higher-resolution satellite imagery have emerged as a possible solution to quantify the distribution of mesquite (Laliberte and Rango 2011; Jackson et al., 2020). The use of conventional red-green-blue (RGB) sensors mounted on a UAV can provide 2-dimensional (2D) and 3-dimensional (3D) products that can be used to better assess woody cover such as measurements of canopy structures, distinguishing different vegetation types, and amount of vegetation cover (Zainuddin et al., 2016; Mayr et al., 2018). LiDAR can provide accurate measurements of canopy volume and height for trees and shrubs, but it still remains relatively costly compared with the data derived from structure from motion (also known as digital aerial photogrammetry) (Iglhaut et al., 2019; Jiang et al., 2020). The functionality of UAVs allows for the generation of imagery at very high spatial resolutions and temporal coverage to map and monitor small patches of vegetation within rangelands that often cannot be captured by satellite imagery (Gonzalez-Dugo et al., 2013; Sankey et al., 2018). Deriving tree heights and land cover area are key components in rangeland monitoring and surveying methods (Wang et al., 2017). Recording tree heights and diameter allows managers the ability to monitor growth of the plant species, calculate the volume of the plant, and calculate forage biomass, and it can aid in determining available habitat for wildlife species (Ivosevic et al., 2015; Zainuddin et al., 2016; Guo et al., 2017; Manfreda et al., 2018; Zhang et al., 2018). Laliberte et al., (2010) were able to perform rangeland inventory assessments to monitor rangelands in Southern Idaho using UAVs with a hierarchical classification process to distinguish different features and vegetation types within the landscape. Rossi et al., (2018) were able to more accurately delineate degraded forests in northern Argentina using a combination of UAV imagery and satellite imagery.

New remote sensing approaches allow the combination of UAV imagery as training datasets for satellite imagery (Puliti et al., 2018; Kattenborn et al., 2019). The information acquired by UAVs can be used to inform lower-resolution imagery (e.g., Sentinel-2) to

improve image classification and combine high spatial resolution imagery with high spectral resolution images to map and quantify the distribution of woody cover species (Rossi et al., 2018; Kattenborn et al., 2019). Puliti et al., (2018) used a combination of UAV and Sentinel-2 imagery to estimate forest growing stock volume in southeastern Norway using hierarchical model-based inference. Images acquired from UAVs have been used as training data for Sentinel satellite imagery to identify three invasive woody cover species (Kattenborn et al., 2019) and detect riparian vegetation with an emphasis on riparian forest habitats (Daryaei et al., 2020). These new technological advances can help improve our ability to assess the spatial distribution of woody encroachment in rangelands and provide additional tools in the natural resource manager's toolbox for planning and adaptive management (Laliberte et al., 2010; Manfreda et al., 2018; Al-Najjar et al., 2019).

The goal of this project was to assess the presence and spatial distribution of mesquite derived from two different remote sensing sources. The specific objectives were 1) evaluate the accuracy of using UAV-based approaches to estimate mesquite height and 2) classify mesquite vegetation presence using a combination of height metrics and spectral information by integrating UAV training data and Sentinel-2 remote sensing data.

Methods

Study sites

This study was conducted in three study areas: a private ranch in Hood County, Texas; a private ranch in Jim Hogg County, Texas; and a property owned by Texas A&M University-Kingsville (hereafter "South Pasture") located in Kleberg County, Texas (**Fig. 1**).

The Hood County ranch lies within the western Cross Timbers ecoregion (Gould 1962). Annual rainfall on the property ranges from 660 to 1 016 mm, and annual temperatures range from 11°C to 25°C (US Climate Data 2020b, Granbury, TX). The topography of this area is hilly with varying elevation change that ranges from 259 m to 305 m above sea level (a.s.l.). The soils in the area are mostly composed of loam, which makes up 47% of the land area, followed by silty clay soils comprising 42% of the area, and the other 11% is comprised of mixed complexes (Web Soil Survey 2020b). The dominant woody species are oaks (genus *Quercus*) and mesquite; the dominant forb is Engelmann's daisy *(Engelmannia peristenia),* and the dominant grasses are little bluestem *(Schizachyrium scoparium)* and sideoats grama *(Bouteloua curtipendula)* (see Table S1, available online at 10.1016/j.rama.2022.03.007 …, for the complete list).

The Jim Hogg County ranch lies within the western portion of the Coastal Sand Plain ecoregion in South Texas (**Fig. 1**; Fulbright et al., 1990). The annual rainfall for the property is 500–800 mm (Mata et al., 2018; Walther 2019) and has annual temperatures ranging from 16°C to 29°C (US Climate Data 2020a, Hebbronville, TX). Elevation at the site is 156 m a.s.l., and the topography is relatively flat. The soils consist mostly of the Delmita and Bruni series, which make up 43% of the area, followed by Delmita fine sandy loam series (40%) and the Nueces-Sarita association (17%) (Web Soil Survey 2020a). The dominant woody species is mesquite, the dominant forb is hoary milkpea *(Galactia canescens),* and the dominant grasses are tanglehead *(Heteropogon contortus)* and coastal sandbur *(Cenchrus spinifex)* (see Table S2, available online at …, for the complete list).

The South Pasture property also lies within the South Texas Plains ecoregion (see Fig. 1; Gould 1962). The average annual rainfall at the site is 736 mm, with annual temperatures ranging from 15°C to 28°C (US Climate Data 2020c, Kingsville, TX). Elevation at the site is 18 m a.s.l., and the topography is relatively flat. Soils on the site consist mostly of sandy clay loams and loamy fine sand, which both account for 25% of the area, respectively, along with Palobia-Colmena complex (22%), clay loams (14%), and river wash (14%) from the creek that runs through the middle of the property (Web Soil Survey 2020c). The dominant woody species are mesquite and lime prickly ash *(Zanthoxylum fagara),* the dominant forbs are woolly croton *(Croton capitatus)* and Texas lantana *(Lantana horrida),* and the dominant grasses are King Ranch bluestem *(Bothriochloa ischaemum)* and bufflegrass *(Pennisetum ciliare)* (see Table S3, available online at 10.1016/j.rama.2022.03.007, for the complete list).

Data collection

We collected UAV data at two altitudes: 50 m and 100 m above ground level (AGL). All UAV flights took place on sunny, clear days, with winds < 16 km • h^{-1}. We used a DJI Phantom IV UAV (SZ DJI Technology Co. Shenzhen, China) for Hood County and a DJI Phantom IV RTK UAV (SZ DJI Technology Co. Shenzhen, China) for Jim Hogg County and South Pasture. The DJI Phantom IV has an integrated GPS/GLONASS system (Global Positioning System/GLObal NAvigation Satellite System), allowing for faster, more precise satellite acquisition during flights, and the DJI Phantom IV RTK connects to a mobile base station that allows images to be geocoded to a higher georeferenced accuracy (1.2 cm relative horizontal accuracy) during flight. Both UAV units were equipped with a 2.5-cm, 20-megapixel camera mounted to a gimbal that stabilizes the camera with the movement of the UAV (pitch, roll, and yaw). Image data collection in Hood County was conducted on June 27, 2019 and consisted of 7 flight missions having a total flight area of 70 ha, 17 ha of which were used for model training and height analysis. Image acquisition at the Jim Hogg County ranch consisted of 2 flight missions on November 6, 2020, encompassing a flight area of 142 ha, with 46 ha used for model training and height analysis. The UAV flights at South Pasture occurred on October 14, 2020 and consisted of 2 flight missions, with a total flight area of 144 ha, 42 ha of which were used for model training and height analysis.

Natural color UAV images (red, green, and blue bands) were acquired with a double-grid flight pattern, at a speed of 3–5 km • h^{-1}, at 70° camera angle, and with 80% image overlap (DiMaggio et al., 2020). We chose these parameters to improve the 3D model by having oblique images to capture the vertical structure of mesquite. We used the Pix4D capture application (Pix4D Inc., San Francisco, CA) for Android for the DJI Phantom IV and the DJI Pilot application (SZ DJI Technology Co. Shenzhen, China) for the DJI Phantom IV RTK. We did not use ground control points (GCPs) in our flight missions, which provided us the opportunity to compare the two UAVs georeferenced accuracies without additional input from georeferenced points.

For each study site, we located pastures that had mesquite trees present and used ArcGIS Pro v. 2.5 (ESRI, The Redlands, CA; hereafter "ArcGIS Pro") to create 10 random points that fell within each pasture. In the field, we navigated to each of these points and created a 22.86-m buffer area. Within the buffer area, we measured every mesquite tree's canopy height and its location (Klimas et al., 2004) using a Trimble R1 GPS unit (50-cm accuracy). The buffer area size was chosen on the basis of current Natural Resource Conservation Service practices for quantifying mesquite in rangelands (D. Daniels, unpublished data). To measure the canopy heights, we used a telescoping measuring rod and recorded each height and unique ID number for each mesquite/GPS point location. We then co-located the GPS points with the UAV imagery to identify mesquite trees and delineate mesquite presence and heights.

We acquired Sentinel-2 imagery for each study site (Hood County, Jim Hogg County, and South Pasture) from the US Geological Survey's Earth Explorer (USGS, Reston, VA; https://earthexplorer.usgs.gov). Sentinel-2 imagery captures data in 13

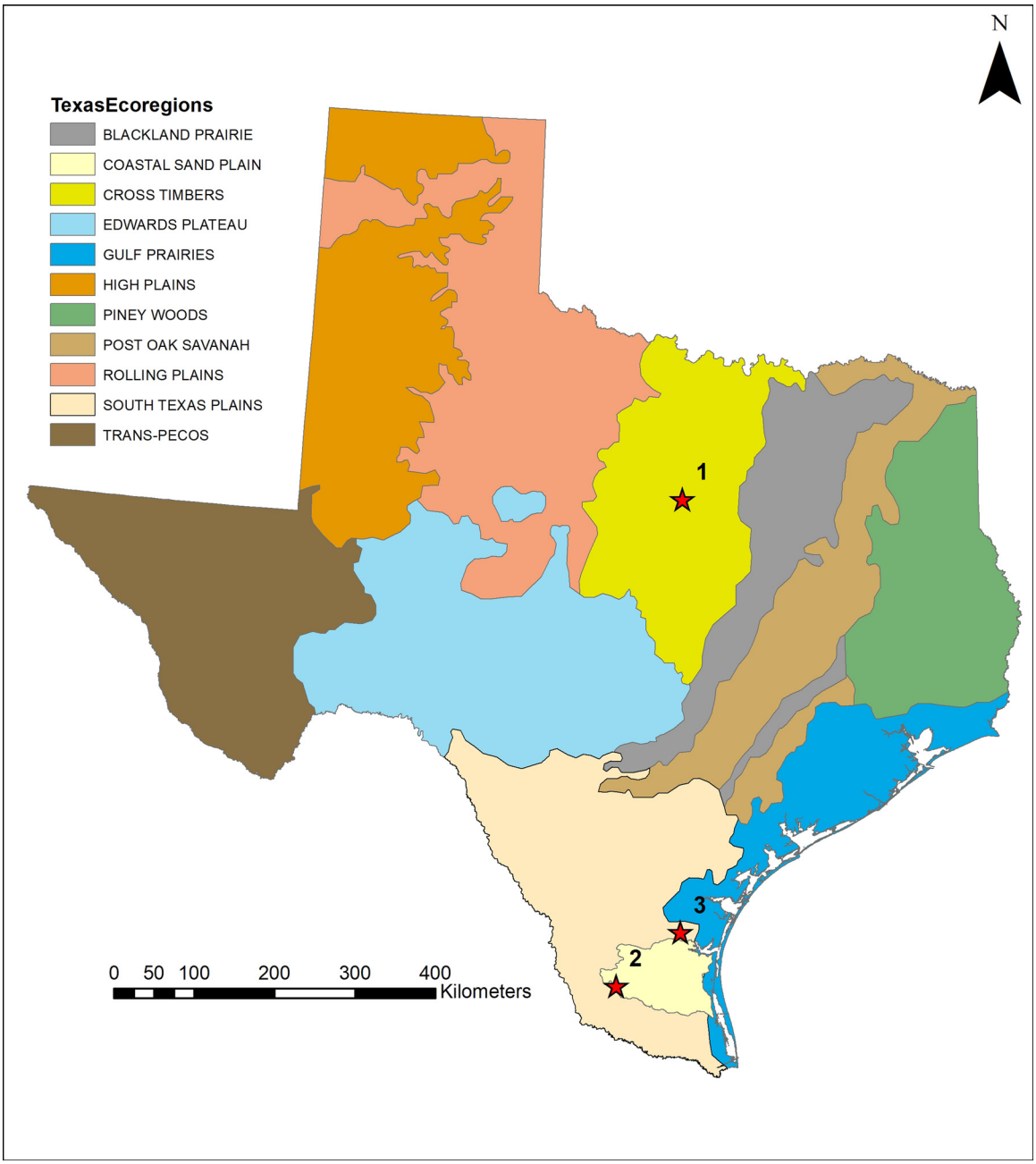

Fig. 1. Study sites locations: Hood Co. is in the Cross Timbers ecoregion *(1);* Jim Hogg Co. is in the Coastal Sand Plain ecoregion *(2);* and South Pasture is in South Texas Plains ecoregion *(3)* (Gould 1962; Fulbright et al., 1990).

bands: red, green, blue, and 1 near infrared bands at 10-m resolution; 3 red edge bands, 1 narrow near infrared band, and 2 shortwave infrared bands at 20-m resolution; and coastal aerosol, water vapor, and shortwave infrared/cirrus bands at 60-m resolution (ESA 2021). We selected cloud-free imagery collected nearest the date of UAV data acquisition. We acquired one scene on June 29, 2019 for Hood County; one scene on October 31, 2020 for Jim Hogg County; and one scene on November 17, 2020 for South Pasture.

Data processing and analysis

We used convergent image networks to develop photogrammetric models using structure-from-motion (SfM), which helped improve model reconstruction accuracy (Cunliffe et al., 2016; Sanz-Ablanedo et al., 2018) for UAV imagery collected at each site. The SfM photogrammetry approach in Pix4D Mapper (Pix4D SA, Switzerland) allowed us to stitch overlapping images captured from the UAV to create and model our 2D orthomosaics, 3D photogrammetric meshes, and 3D point cloud datasets (LAS format) using structured algorithms (Cunliffe et al., 2016; Zainuddin et al., 2016; Liu et al., 2018; Al-Najjar et al., 2019). These 2D (e.g., orthoimagery) and 3D (point cloud data) outputs can be used to model canopy height and volume along with 3D photorepresentation of landscapes (Cunliffe et al., 2016). We used two methods of evaluating canopy height from the UAV: the Vertical Measurement Tool (VMT; ESRI 2021a) in ArcGIS Pro and the LAS Point Cloud height metric output (ESRI 2021b). We compared both UAV-derived height methods to field-collected canopy height data to assess the perfor-

mance of each approach. We also compared root mean square error (RMSE) of the geolocation accuracy for each UAV flight (Pix4D SA, Switzerland).

VMT

We used the mesquite GPS locations in the 3D photogrammetric mesh to identify individual mesquite trees ($n = 81$ in Hood County, $n = 46$ in Jim Hogg County, and $n = 41$ in Kleberg County) in ArcScene (ArcGIS Pro). For each tree, we used the VMT in ArcGIS Pro (ESRI 2021a) to measure from the base of the mesquite tree to the crown and recorded the height value.

LAS Point Cloud

We verified that ground points in the dataset were properly assigned by using the Classify LAS Ground tool (ESRI 2021b). We calculated heights of objects within the image, assigned a minimum height value to 0.5 m, and rescaled cell size to 0.2 m with the LAS Height Metrics tool (ESRI 2021c). We exported this output as a 2D LAS height raster that we used to record individual tree height values (Zainuddin et al., 2016). We used the GPS location points to identify the mesquite trees to digitize the canopy crowns (Mayr et al., 2018). We used the 2D LAS height raster layer and digitized mesquite layer as an input to receive an output of the maximum height for each shape using the zonal statistics tool (ESRI 2021d). This value represented mesquite tree heights, which were compared with field-recorded values (Mayr et al., 2018).

Regression analysis

We performed linear regressions to examine the relationship between field-collected variables and the UAV-derived outputs produced by the VMT and the LAS height metrics layer using NCSS statistical software (NCSS, LLC, Kaysville, UT). Linear regressions were performed on both 50-m altitude flights and 100-m altitude flights for each of the three study sites. We compared coefficients of determination and residuals (e.g., RMSEs) of the linear models following methods described by Graybill (Graybill 1976). To verify the models, we calculated the prediction coefficients of determination (prediction r^2) along with PRESS statistics (Montgomery et al., 2012; DiMaggio et al., 2020).

Scaling from UAV to satellite imagery

We used the UAV-derived products (2D orthomosaic and 3D point-cloud dataset) to classify mesquite. On the basis of height and individual identification of mesquite trees based on GPS data collected in the field, we created a classified image from the UAV orthomosaic with two classes, "mesquite" and "not-mesquite." The spectral information (red, green, and blue) alone did not provide enough information to separate mesquite from other types of land cover. We used random forest machine learning techniques to quantify amount of mesquite cover within the landscape from the UAV-derived products. Machine learning is the use of artificial intelligence to perform tasks not explicitly programmed by humans (Ghahramani 2015). To delineate "not-mesquite," we digitized various features in the imagery such as roads, water, and other vegetation at a scale of 1:50 in ArcGIS Pro 2.x (ESRI, the Redlands). We then used the pixel boundaries of the Sentinel-2 imagery to create a 10-m fishnet polygon grid within the area of the UAV orthomosaic. If mesquite is present in the fishnet, we included it as present. We input mesquite presence from the fishnet grid to inform classification of Sentinel-2 satellite imagery (Kattenborn et al., 2019). We used the random forest classification to perform the conversion analysis (Al-Najjar et al., 2019; Kattenborn et al., 2019; ESRI 2021e.). For our input layers, we used Sentinel-2 bands 2-8, 8a, 11, and 12 (Kattenborn et al., 2019; Jensen et al., 2020). We excluded bands 1, 9, and 10 because of coarse spatial resolutions (60 m) and because their purposes did not match our objectives as these coarse bands are primarily used for cloud screening and atmospheric corrections (Kattenborn et al., 2019; ESA 2021). We used 80% of our training data for model training and 20% for verification of the model (Kattenborn et al., 2019).

Accuracy assessments of mesquite presence classification were performed using a confusion matrix and kappa statistics (Landis and Koch 1977; Carfagna and Gallego 2005; Ng et al., 2017). To perform the accuracy assessment, we created 200 random points across each study site with a 10-m minimum distance required between points. We implemented this minimum distance to prevent multiple points from falling in the same square of the fishnet grid. Using the 10-m fishnet and high-resolution UAV imagery, we verified the presence or lack of mesquite within the 10-m fishnet pixel. We compared overall accuracy, user's accuracy, and producer's accuracy values using a confusion matrix (Landis and Koch 1977; Story and Congalton 1986; Carfagna and Gallego 2005; Shao et al., 2019). Overall accuracy refers to the number of pixels classified correctly versus the total number of pixels used for the accuracy assessment (Congalton 1991). The producer's accuracy refers to the number of correctly classified pixels divided by the total number of reference pixels for each category. The user's accuracy refers to the number of correctly classified pixels divided by the total number of classified pixels for each category. We calculated kappa statistics (ranged 0–1) to represent differences between actual agreement, reference data, and the classification classifier in comparison with the likelihood of agreement between a random classifier and reference data (Landis and Koch 1977; Adam et al., 2017).

Results

Pixel resolutions ranged from 1.71 cm^2 to 2.4 cm^2 for the 50-m AGL flights and 3.39 cm^2 to 4.76 cm^2 for the 100-m AGL flights (Table 1). Geolocation RMSE values were higher in the imagery acquired from the DJI Phantom IV when compared with the DJI Phantom IV RTK (see Table 1). For both the VMT and the LAS height estimations, the 50 m AGL Hood County site had the highest r^2 values out of all the sites with ($r^2 = 0.95$, RMSE = 24.9 and 26.6 cm) (Fig. 2). The 100-m AGL Hood County site also had the highest r^2 values out of the 100-m AGL flights ($r^2 = 0.91$, RMSE = 32.3 cm for the VMT; $r^2 = 0.92$, RMSE = 29.6 cm for the LAS). The estimated mesquite heights from the 50-m AGL flight corresponded more closely to the field-measured heights than those estimates from the 100-m AGL flight for both height estimation methods ($r^2 = 0.884$ vs. $r^2 = 0.758$, respectively, for the VMT; $r^2 = 0.796$ vs. $r^2 = 0.764$, respectively, for the LAS; see Fig. 2). The Jim Hogg County site had higher r^2 values for the VMT at 50-m AGL than 100-m AGL ($r^2 = 0.851$ and $r^2 = 0.587$, respectively, and lower r^2 values with LAS at 50-m AGL than 100-m AGL ($r^2 = 0.827$ and $r^2 = 0.857$, respectively). We found that the Hood County site had regression RMSE values that ranged from 24.9 cm to 32.3 cm, and the other two sites had average errors that ranged from 54.7 cm to 93 cm (Table 2). Differences between r^2 values and prediction r^2 values for the different height analysis and sites ranged from 0.0022 to 0.0452, and PRESS statistics were 5–18% higher than corresponding original error sum of squares values for the height analysis (see Table 2).

Overall accuracy assessment of mesquite presence derived from Sentinel-2 satellite imagery (Fig. 3) was > 80% for all three study sites (Table 3). The highest accuracy was seen in the South Pasture property with an accuracy of 87.5%, followed by Hood County with 84% and Jim Hogg with 80.5%. The highest values for

Table 1
Unpiloted aerial vehicle (UAV) processing accuracy separated by flight mission; geolocation root mean square error (RMSE) triangulation values in cm from Pix4D photogrammetry software processing.

Flight mission	UAV model	Pixel size (cm)	RMSE X (cm)	RMSE Y (cm)	RMSE Z (cm)
Hood 50m F1		2.35	58.6404	156.5385	36.6762
Hood 50m F2		2.4	124.7067	135.7747	128.7687
Hood 50m F3		1.86	102.4717	51.4863	114.2609
Hood 50m F4	DJI Phantom IV	2.39	131.1338	110.7732	59.3524
Hood 100m F1		4.12	41.8060	61.7831	48.5952
Hood 100m F2		4.66	211.9485	276.2539	53.4396
Hood 100m F3		4.76	134.7223	252.2633	44.5589
Jim Hogg 50 m		1.71	0.2063	0.2254	0.7380
Jim Hogg 100 m	DJI Phantom IV RTK	3.39	0.3310	0.5890	2.4762
South Pasture 50 m		2.22	0.2830	0.3098	0.5966
South Pasture 100 m		4	0.2866	0.2760	0.9154

Table 2
Statistical regression comparisons between unpiloted aerial vehicles (UAV)-derived height methods to field collected canopy height data; root mean square error of regressions (RMSE) in cm; PRESS statistics and predicted r^2 values were computed for model validation; PRESS statistics % difference is the percentage higher the predicted error sum of squares is compared with the original error sum of squares.

Study site	Flight altitude	Height Tool	r^2 value	P value	RMSE (cm)	Prediction r^2(PRESS statistic)	PRESS statistics % difference
Hood	50	LAS	0.9566	$P < .001$	24.9	0.9544	5%
	m	VMT	0.9504	$P < .001$	26.6	0.9468	7.3%
	100	LAS	0.9263	$P < .001$	29.6	0.9129	18%
	m	VMT	0.9120	$P < .001$	32.3	0.8971	17%
Jim	50	LAS	0.8267	$P < .001$	60.2	0.8137	7.5%
Hogg	m	VMT	0.8510	$P < .001$	55.8	0.8380	8.7%
	100	LAS	0.8567	$P < .001$	54.7	0.8443	8.6%
	m	VMT	0.5870	$P < .001$	92.9	0.5418	11%
South	50	LAS	0.7959	$P < .001$	64.8	0.7762	9.7%
Pasture	m	VMT	0.8844	$P < .001$	48.7	0.8748	8.3%
	100	LAS	0.7644	$P < .001$	69.6	0.7398	10.4%
	m	VMT	0.7583	$P < .001$	70.5	0.7295	12%

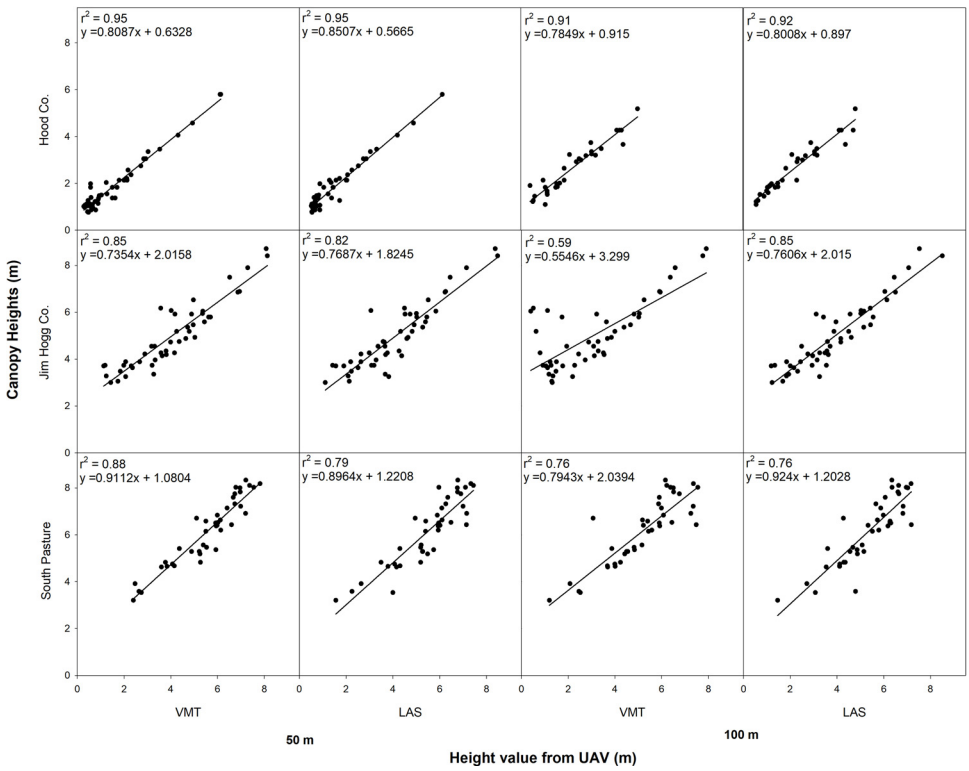

Fig. 2. Canopy height comparison regressions. Rows indicate the three study sites; Y-axis, the field-recorded canopy height measurement; Columns, the combination of unpiloted aerial vehicle (UAV)-derived outputs and altitude differences; X-axis, the UAV-derived canopy height with each of the UAV methods (vertical measurement tool and LAS point cloud raster.

Fig. 3. Image classification of mesquite. From top to bottom: UAV imagery; Sentinel-2 imagery; classified imagery using random forest prediction.

producer and user accuracy were in the South Pasture site (Producer accuracy = 92%; User accuracy = 87%). The Jim Hogg County site yielded lower producer accuracies than the Hood County site (Producer accuracy = 70%; User accuracy = 89%) but higher user accuracies (Producer accuracy = 73%; User accuracy = 60%). The highest Kappa values were observed at South Pasture (K = 0.74), followed by the Hood and Jim Hogg sites (K = 0.61 and K = 0.56).

Discussion

The analysis of UAV-derived canopy height methods provided reliable measures of woody cover vegetation (Mesquite) in Texas rangelands. Our analyses of UAV point cloud data provided reliable measures of mesquite height. Our highest r^2 was 0.95 for both the VMT and LAS height metric (Hood County; 50 m AGL), and our lowest r^2 was 0.587 for VMT (Jim Hogg County 100 m AGL) and

Table 3
Accuracy assessments using confusion matrix results of the three study sites comparing mesquite and other landscape classes; with Overall Accuracy (OA), User Accuracy (UA), Producer Accuracy (PA), and Kappa statistics.

Hood Co.	mesquite	other	Total	UA %	PA %
Mesquite	39	27	66	59.1%	88.6%
Other	5	129	134	96.3%	82.7%
Total	44	156	200		
OA = 84%	Kappa = 0.61				
Jim Hogg Co.					
Mesquite	48	18	66	72.7%	69.5%
Other	21	113	134	84.3%	86.3%
Total	69	131	200		
OA = 80.5%	Kappa = 0.56				
South Pasture					
Mesquite	105	16	121	86.8%	92.1%
Other	9	70	79	88.6%	81.4%
Total	114	86	200		
OA = 87.5%	Kappa = 0.74				

0.764 for the LAS height metric (South Pasture; 100-m AGL). For the Hood County site, prediction errors ranged from ±24 to 32 cm. Errors were larger at the Jim Hogg and South Pasture sites with errors ranging from ±54 to 92 cm. Trees were taller at the Jim Hogg and South Pasture site, which may have increased the prediction error. Our UAV-derived canopy height results were comparable with other studies (Zarco-Tejada et al., 2014; Wallace et al., 2016; Mayr et al., 2018). Mayr et al., (2018) used a UAV at 70-m AGL to record canopy heights of *Acacia mellifera, Dichrostachys cinerea,* and *Terminalia sericea* by subtracting digital terrain models from digital surface models and compared outputs with field-recorded canopy heights, which yielded r^2 values ranging from 0.7 to 0.72. Zarco-Tejada et al., (2014) had r^2 values that ranged between 0.81 and 0.86 when comparing field-measured olive tree heights to digital surface model UAV outputs from a fixed-wing UAV flown at 200-m AGL. Wallace et al., (2016) compared aerial LiDAR- and UAV-derived 3D point cloud heights acquired at 30-m AGL and reported r^2 values of 0.84 (LiDAR) and 0.68 (point cloud). Our results from three different ecoregions in Texas indicate that UAVs could reliably measure mesquite canopy heights to assist in assessing canopy structure.

We found that UAV flight altitude was not critical for the estimation of mesquite tree canopy heights. Prediction errors were similar for each of the flight altitudes evaluated, regardless of location. Our results at 50-m AGL (see Table 2) and 100-m AGL (see Table 2) were similar to Torres-Sánchez et al., (2015), who reported r^2 values of 0.90 at 50-m AGL and 0.84 at 100-m AGL. Our model verification results for tree height estimation (see Table 2) showed that our original models were robust with r^2 differences < 0.05 and PRESS statistic error sum of squares ranging between 5% and 18% higher than the error sum of squares in the original model. Models were more robust for the 50-m AGL flights than the 100-m AGL flights for all study sites; however, the differences in accuracy were relatively minor. Flying UAVs at higher altitude would allow users to cover larger areas for woody vegetation monitoring. Our results indicate that the differences in accuracy between the flight altitudes would not compromise the quality monitoring of mesquite heights.

We found that both UAV models proved to be able to capture accurate representations of the landscape. The DJI Phantom IV RTK provided higher horizontal accuracy (see Table 1) and provided the ability to create single large flight missions rather than multiple small missions. We observed higher r^2 values with the DJI Phantom IV missions at Hood County than at the other two sites. However, the Hood County flights had the higher geolocation RMSE values (see Table 1). The RMSE value, however, was not critical to the analysis because we were still able to identify individual trees that we measured in the field. We observed that mature mesquite trees often had thin branches as the highest point in the canopy, which may not be dense enough to pick up in the SfM analysis, thus resulting in reduced accuracy. Meyer et al., (1971) showed that as mesquite trees grow, most of the new stems grow on the upper branches, making them the smallest and thinnest part of the tree. With taller trees in Jim Hogg County and South Pasture (1 m to > 8 m) compared with Hood County (1–6 m), lower r^2 values could be explained by the presence of these thin branches, which were likely difficult to capture in the SfM analysis.

Our results indicate that UAV imagery can be used as training data for using Sentinel-2 satellite imagery and machine learning (random forest) techniques were useful for developing mesquite presence maps over large areas. Overall accuracy values for the models exceeded 80%, similar to other comparable studies. Ng et al., (2017) reported a user accuracy of 72% and a Producer accuracy of 73% specific to *Prosopis* in Sentinel-2 imagery, which was similar to the results reported in this study (User accuracy = 60–86%; Producer accuracy = 70–92%). Discrepancies with image classification in satellite imagery because of its coarse spatial resolution where single pixels encompass multiple landscape features are a common problem (Ng et al., 2017; Daryaei et al., 2020). To limit model confusion, we classified the presence of mesquite without trying to classify multiple landscape classes. The strength of agreement of our sites were moderate to substantial, with our Kappa values ranging between 0.56 and 0.74 (Landis and Koch 1977). The approaches presented in this study could be extrapolated to other woody plant species on rangelands. Canopy height has been shown to be one of the most important measures to determine woody cover structure and ecological value in rangelands (Zarco-Tejada et al., 2014; Wallace et al., 2016), along with providing insight into wildlife habitat (Hyde et al., 2006; Martinuzzi et al., 2009). Our results could be easily used to quantify the presence and spatial distribution of other woody plant species to quantify the amount of cover in the landscape. These methods, used in combination with time-series data, could provide useful baselines for monitoring change and spatial structure of woody cover in rangelands (Rhodes et al., 2021).

Combining high spatial resolution of UAV imagery with Sentinel-2 satellite imagery could assist with future monitoring of mesquite in rangelands. Past remote sensing methods have spatial, spectral, and/or temporal resolution limitations (Mata et al., 2018). Recent advances in satellite and UAV imagery are providing new opportunities to meet these needs. Adam et al., (2017) used a different approach than our study to classify mesquite and other landscape classes by performing random forest classification and support vector machine on World View-2 satellite imagery (1.5–2

m spatial resolution). Although they produced higher user and producer accuracies with mesquite than our results (User accuracy = 96%; Producer accuracy = 100%), this could be attributed to the higher spatial resolution (2 m vs. 10 m) or number of accuracy assessment points to study size area (164 points for 4 795 ha vs. 200 points for < 150 ha; Shao et al., 2019). Their overall accuracy (overall accuracy = 86%), however, is comparable with our results (see Table 3). Further research needs to address point density for accuracy assessment and area coverage to validate UAV classification with lower-resolution imagery.

The analysis of UAV-derived canopy height methods provided reliable measures of mesquite height in Texas. We found that the UAV flight altitude was not critical between 50 m and 100 m AGL for the estimation of mesquite tree canopy heights. We also found that using machine learning techniques, UAV imagery can be used as training data for Sentinel-2 satellite imagery to produce landscape maps of mesquite presence. Being able to combine the high spatial resolution of the UAV imagery with the high temporal resolution of the Sentinel-2 satellite imagery could improve our ability to use UAVs to monitor mesquite in rangelands. Our findings show the potential use of UAV to effectively link information on the ground, UAV-derived products, and satellite imagery for a wider variety of applications. Similar approaches can be used to determine the presence of other woody cover species in different ecosystems. The development of new multispectral cameras can provide opportunities to identify woody cover species and use fractional cover analysis to determine the cover of different species across the landscape by upscaling the information to satellite imagery. Additional spectral, temporal, and spatial resolution (e.g., next-generation Planetscope imagery) combined with UAV products present new opportunities to efficiently quantify and monitor land cover and land cover changes at scales that were not possible a few years ago.

Implications

Our study showed that UAVs can be used to efficiently assess mesquite height in rangelands in different ecoregions of Texas. These heights can provide valuable information for management decisions for woody plant encroachment. Having height metrics can also assist with determining habitat for wildlife species. Our regions of interest were limited by UAV capability to collect data (i.e., battery time), so we tested our approach in three different study areas, which provided more generalizable approaches to assess the amount mesquite presence. These assessments can be used to quantify the presence and spatial distribution of mesquite and potentially other woody plant species to help develop strategies for woody plant management in rangelands. The methods described in this study also show possibilities for managers to assess wildlife habitat, conduct rangeland inventories, and establish baselines to prioritize ecological management strategies.

Declaration of Competing Interest

The authors declare that they have no known competing financial interests or personal relationships that could have appeared to influence the work reported in this paper.

Acknowledgments

We are very grateful to the landowners who provided access to their land so that we could achieve the goals of our project. We want to thank H. Su and J. Baumgardt for the comments and suggestions and the 2 anonymous reviewers who helped improve this manuscript.

Supplementary materials

Supplementary material associated with this article can be found, in the online version, at doi:10.1016/j.rama.2022.03.007.

References

Adam, E., Mureriwa, N., Newete, S., 2017. Mapping *Prosopis glandulosa* (mesquite) in the semi-arid environment of South Africa using high-resolution WorldView-2 imagery and machine learning classifiers. Journal of Arid Environments 145, 43–51.

Addabbo, P., Focareta, M., Marcuccio, S., Votto, C., Ullo, S.L, 2016. Contribution of Sentinel-2 data for applications in vegetation monitoring. ACTA IMEKO 5, 44.

Al-Najjar, H.A.H., Kalantar, B., Pradhan, B., Saeidi, V., Halin, A.A., Ueda, N., Mansor, S., 2019. Land cover classification from fused DSM and UAV images using convolutional neural networks. Remote Sensing 11, 1461.

Anderson, M. K., and Roderick, W. 2003. Honey mesquite, USDA NRCS plant guide. Available at: https://plants.usda.gov/plantguide/pdf/cs_prglt.pdf. Accessed 22 October, 2020.

Ansley, R.J., Huddle, J.A., Kramp, B.A., 1997. Mesquite ecology. Texas Natural Resources Server. Available at https://texnat.tamu.edu/library/symposia/brush-sculptors-innovations-for-tailoring-brushy-rangelands-to-enhance-wildlife-habitat-and-recreational-value/mesquite-ecology/ . Accessed 22 October, 2020.

Ansley, R.J., Wu, X.B., Kramp, B.A, 2001. Observation: long-term increases in mesquite canopy cover in a North Texas savanna. Journal of Range Management 54, 171–176.

Ansley, R.J., Zhang, T., Cooper, C, 2018. Soil moisture, grass production and mesquite resprout architecture following mesquite above-ground mortality. Water 10, 1243.

Archer, S., Stokes, C., 2000. Stress, disturbance and change in rangeland ecosystems. In: Arnalds, O., Archer, S. (Eds.), Rangeland desertification. Springer, The Netherlands, pp. 17–38.

Archer, S., Boutton, T.W., Hibbard, K.A, 2001. Trees in grasslands: biogeochemical consequences of woody plant expansion. Academic Press, San Diego, CA, USA, pp. 115–137.

Archer, S.R., 2010. Rangeland conservation and shrub encroachment: new perspectives on an old problem. In: du Toit, J.T., Kock, R., Deutsch, J. (Eds.), Wild rangelands: conserving wildlife while maintaining livestock in semi-arid ecosystems. John Wiley & Sons, Ltd, Hoboken, NJ, USA, pp. 53–97.

Ball, L., and Taylor, M. 2003. Brush management: myths and facts. Environmental defense. Available at: http://texaslivingwaters.org/wp-content/uploads/2013/04/tlw-brush_management-03.pdf. Accessed 12 October, 2020.

Carey, M.P., Sanderson, B.L., Barnas, K.A., Olden, J.D, 2012. Native invaders–challenges for science, management, policy, and society. Frontiers in Ecology and the Environment 10, 373–381.

Carfagna, E., Gallego, F.J, 2005. Using remote sensing for agricultural statistics. International Statistical Review 73, 389–404.

Congalton, R.G., 1991. A review of assessing the accuracy of classifications of remotely sensed data. Remote Sensing of Environment 37, 35–46.

Cunliffe, A.M., Brazier, R.E., Anderson, K, 2016. Ultra-fine grain landscape-scale quantification of dryland vegetation structure with drone-acquired structure-from-motion photogrammetry. Remote Sensing of Environment 183, 129–143.

Dahl, B.E., 1982. Mesquite as a rangeland plant. In: Parker, H.W. (Ed.), Mesquite utilization. Texas Tech University, Lubbock, TX, USA, pp. 1–20.

Daryaei, A., Sohrabi, H., Atzberger, C., Immitzer, M., 2020. Fine-scale detection of vegetation in semi-arid mountainous areas with focus on riparian landscapes using Sentinel-2 and UAV data. Computers and Electronics in Agriculture 177, 0168–1699.

DiMaggio, A.M., Perotto-Baldivieso, H.L., Ortega-S, J.A., Walther, C., Labrador-Rodriguez, K.N., Page, M.T., Martinez, J.L., Rideout-Hanzak, S., Hedquist, B.C., Wester, D.B, 2020. A pilot study to estimate forage mass from unmanned aerial vehicles in a semi-arid rangeland. Remote Sensing 12, 2431.

Dos Reis, A.A., Werner, J.P.S., Silva, B.C., Figueiredo, G.K.D.A., Antunes, J.F.G., Esquerdo, J.C.D.M., Coutinho, A.C., Lamparelli, R.A.C., Rocha, J.V., Magalhães, P.S.G., 2020. Monitoring pasture aboveground biomass and canopy height in an integrated crop–livestock system using textural information from PlanetScope imagery. Remote Sensing 12, 2534.

Drusch, M., Gascon, F., and Berger, M. 2010. Sentinel-2 Mission Requirements Document (2), 42. Available at: https://earth.esa.int/web/guest/-/gmes-sentinel-2-mission-requirements-6440. Accessed 4 January, 2021.

ESA. 2021. Sentinel-2: The European Space Agency. Available at: https://sentinel.esa.int/web/sentinel/missions/sentinel-2/. Accessed 04 January, 2021.

ESRI. 2021a. Measure. Available at: https://pro.arcgis.com/en/pro-app/latest/help/mapping/navigation/measure.htm. Accessed 05 January, 2021.

ESRI. 2021b. Classify LAS ground: 3D analyst. Available at: https://pro.arcgis.com/en/pro-app/latest/tool-reference/3d-analyst/classify-las-ground.htm. Accessed 05 January, 2021.

ESRI. 2021c. LAS height metrics: 3D analyst. Available at: https://pro.arcgis.com/en/pro-app/latest/tool-reference/3d-analyst/las-height-metrics.htm. Accessed 05 January, 2021.

ESRI. 2021d. How zonal statistics works. Available at: https://pro.arcgis.com/en/pro-app/latest/tool-reference/spatial-analyst/how-zonal-statistics-works.htm. Accessed 05 January, 2021.

ESRI. 2021e. Forest-based classification and regression: spatial statistics. Available at: https://pro.arcgis.com/en/pro-app/latest/tool-reference/spatial-statistics/forestbasedclassificationregression.htm. Accessed 08 January, 2021.

Fang, H., Liang, S., McClaran, M.P., van Leeuwen, W.J.D., Drake, S., Marsh, S.E., Thomson, A.M., Izaurralde, R.C., Rosenberg, N.J, 2005. Biophysical characterization and management effects on semiarid rangeland observed from Landsat ETM+ data. IEEE Transactions in Geoscience. Remote Sensing 43, 125–134.

Fulbright, T.E., Diamond, D.D., Rappole, J., Norwine, J., 1990. The coastal sand plain of Southern Texas. Rangelands 12, 337–340.

Ghahramani, Z., 2015. Probabilistic machine learning and artificial intelligence. Nature 521, 452–459.

Gillan, J.K., McClaran, M.P., Swetnam, T.L., Heilman, P., 2019. Estimating forage utilization with drone-based photogrammetric point clouds. Rangeland Ecology & Management 72, 575–585.

Gonzalez-Dugo, V., Zarco-Tejada, P., Nicolás, E., Nortes, P.A., Alarcón, J.J., Intrigliolo, D.S., Fereres, E., 2013. Using high resolution UAV thermal imagery to assess the variability in the water status of five fruit tree species within a commercial orchard. Precision Agriculture 14, 660–678.

Gould, F.W., 1962. Texas plants: a checklist and ecological summary. The Agricultural and Mechanical College of Texas, Texas Agricultural Experiment Station, College Station, TX, USA, p. 112.

Graybill, F., 1976. Theory and application of the linear model. Duxberry Press, North Scituate, MA, USA.

Guo, X., Coops, N.C., Tompalski, P., Nielsen, S.E., Bater, C.W., Stadt, J.J, 2017. Regional mapping of vegetation structure for biodiversity monitoring using airborne LiDAR data. Ecological Informatics 38, 50–61.

Heaton, C.B., Wu, X.B., Ansley, R.J, 2003. Herbicide effects on vegetation spatial patterns in a mesquite savanna. Journal of Range Management 56, 627–633.

Hennessy, J.T., Gibbens, R.P., Tromble, J.M., Cardenas, M., 1983. Vegetation changes from 1935 to 1980 in mesquite dunelands and former grasslands of Southern New Mexico. Journal of Range Management 36, 370–374.

Huxman, T.E., Wilcox, B.P., Breshears, D.D., Scott, R.L., Snyder, K.A., Small, E.E., Hultine, K., Pockman, W.T., Jackson, R.B, 2005. Ecohydrological implications of woody plant encroachment. Ecology 86, 308–319.

Hyde, P., Dubayah, R., Walker, W., Blair, J.B., Hofton, M., Hunsaker, C., 2006. Mapping forest structure for wildlife habitat analysis using multi-sensor (LiDAR, SAR/InSAR, ETM+, Quickbird) synergy. Remote Sensing of Environment 102, 63–73.

Iglhaut, J., Cabo, C., Puliti, S., Piermattei, L., O'Connor, J., Rosette, J, 2019. Structure from motion photogrammetry in forestry: a review. Current Forestry Reports 5, 155–168.

Ivosevic, B., Han, Y.G., Cho, Y., Kwon, O., 2015. The use of conservation drones in ecology and wildlife research. Journal of Ecology and the Environment 38, 113–118.

Jackson, M., Portillo-Quintero, C., Cox, R., Ritchie, G., Johnson, M., Humagain, K., Subedi, M.R, 2020. Season, classifier, and spatial resolution impact honey mesquite and yellow bluestem detection using an unmanned aerial system. Rangeland Ecology & Management 73, 658–672.

Jensen, T., Hass, F.S., Akbar, M.S., Petersen, P.H., Arsanjani, J.J, 2020. Employing machine learning for detection of invasive species using sentinel-2 and AVIRIS data: the case of kudzu in the United States. Sustainability 12, 3544.

Jiang, S., Jiang, C., Jiang, W., 2020. Efficient structure from motion for large-scale UAV images: a review and a comparison of SfM tools. ISPRS Journal of Photogrammetry and Remote Sensing 167, 230–251.

Kattenborn, T., Lopatin, J., Förster, M., Braun, A.C., Fassnacht, F.E, 2019. UAV data as alternative to field sampling to map woody invasive species based on combined Sentinel-1 and Sentinel-2 data. Remote Sensing Environment 227, 61–73.

Klimas, C. V., Murray, E. O., Pagan, J., Langston, H., and Foti, T. 2004. A regional guidebook for applying the hydrogeomorphic approach to assessing wetland functions of forested wetlands in the delta region of Arkansas, lower Mississippi River Alluvial Valley. Ecosystem Management and Restoration Research Program. Appendix A3. Available at: https://wetlands.el.erdc.dren.mil/pdfs/trel04-16.pdf. Accessed 17 February, 2021.

Ku, N.W., Popescu, S.C., Ansley, R.J., Perotto-Baldivieso, H.L., Filippi, A.M, 2012. Assessment of available rangeland woody plant biomass with a terrestrial LiDAR system. Photogrammetric Engineering and Remote Sensing 78, 349–361.

Laliberte, A.S., Herrick, J.E., Rango, A., Winters, C., 2010. Acquisition, orthorectification, and object-based classification of unmanned aerial vehicle (UAV) imagery for rangeland monitoring. Photogrammetric Engineering and Remote Sensing 76, 661–672.

Laliberte, A.S., Rango, A., 2011. Image processing and classification procedures for analysis of sub-decimeter imagery acquired with an unmanned aircraft over arid rangelands. GISci. Remote Sensing 48, 4–23.

Landis, J.R., Koch, G.G, 1977. The measurement of observer agreement for categorical data. Biometrics 33, 159–174.

Liu, Y., Zheng, X., Ai, G., Zhang, Y., Zuo, Y., 2018. Generating a high-precision true digital orthophoto map based on UAV images. ISPRS International Journal of Geo-Inf 7, 333.

Manfreda, S., McCabe, M.F., Miller, P.E., Lucas, R., Madrigal, V.P., Mallinis, G., Dor, E.B., Helman, D., Estes, L., Ciraolo, G., Müllerová, J., Tauro, F., De Lima, M.I., De Lima, J.L.M.P., Maltese, A., Frances, F., Caylor, K., Kohv, M., Perks, M., Ruiz-Pérez, G., Su, Z., Vico, G., Toth, B., 2018. On the use of unmanned aerial systems for environmental monitoring. Journal of Remote Sensing 10, 641.

Martinuzzi, S., Vierling, L.A., Gould, W.A., Falkowski, M.J., Evans, J.S., Hudak, A.T., Vierling, K.T, 2009. Mapping snags and understory shrubs for a LiDAR-based assessment of wildlife habitat suitability. Remote Sensing Environment 113, 2533–2546.

Mata, J.M., Perotto-Baldivieso, H.L., Hernández, F., Grahmann, E.D., Rideout-Hanzak, S., Edwards, J.T., Page, M.T., Shedd, T.M, 2018. Quantifying the spatial and temporal distribution of tanglehead *(Heteropogon contortus)* on south Texas rangelands. Ecological Processes 7, 2.

Mayr, M.J., Malß, S., Ofner, E., Samimi, C., 2018. Disturbance feedbacks on the height of woody vegetation in a savannah: a multi-plot assessment using an unmanned aerial vehicle (UAV). International Journal of Remote Sensing 39, 4761–4785.

Meyer, R. E., Morton, H. L., Haas, R. H., Robison, E. D., and Riley, T. E. 1971. Morphology and anatomy of honey mesquite. ARS USDA Technical Bulletin No. 1423. Available at: https://naldc.nal.usda.gov/download/CAT71318019/PDF. Accessed 10 October, 2020.

Mirik, M., Ansley, R.J., 2012. Utility of satellite and aerial images for quantification of canopy cover and infilling rates of the invasive woody species honey mesquite *(Prosopis glandulosa)* on rangeland. Remote Sensing 4 1947−1962.

Mohamed, A.H., Holechek, J.L., Bailey, D.W., Campbell, C.L., DeMers, M.N, 2011. Mesquite encroachment impact on southern New Mexico rangelands: remote sensing and geographic information systems approach. Journal of Applied Remote Sensing 5, 1.

Montgomery, D.C., Peck, E.A., Vining, G.G, 2012. Introduction to linear regression analysis, 5th ed.. John Wiley & Sons, Inc, Hoboken, NJ, USA, p. 672.

Musick, H.B., 1984. Assessment of Landsat multispectral scanner spectral indexes for monitoring arid rangeland. IEEE Transactions in Geoscience Remote Sensing 22, 512–519.

Ng, W.T., Rima, P., Einzmann, K., Immitzer, M., Atzberger, C., Eckert, S., 2017. Assessing the potential of Sentinel-2 and Pléiades data for the detection of *Prosopis* and *Vachellia* spp. in Kenya. Remote Sensing 9, 74.

Nie, W., Yuan, Y., Kepner, W., Erickson, C., Jackson, M, 2012. Hydrological impacts of mesquite encroachment in the upper San Pedro watershed. Journal of Arid Environments 82, 147–155.

NRCS. Plants Database. 2020. *Prosopis glandulosa*. Available at: https://plants.sc.egov.usda.gov/core/profile?symbol=PRGL2. Accessed 15 April, 2020.

Puliti, S., Saarela, S., Gobakken, T., Ståhl, G., Næsset, E., 2018. Combining UAV and Sentinel-2 auxiliary data for forest growing stock volume estimation through hierarchical model-based inference. Remote Sensing Environment 204, 485–497.

Ratajczak, Z., Nippert, J.B., Collins, S.L., 2012. Woody encroachment decreases diversity across North American grasslands and savannas. Ecology 93, 697–703.

Rhodes, E.C., Angerer, J.P., Fox, W.E., McAlister, J.R, 2021. Woody vegetation cover, attrition, and patch metrics over eight decades in central Texas, United States. Rangeland Ecology & Management 78, 54–66.

Rossi, F.C., Fritz, A., Becker, G., 2018. Combining satellite and UAV imagery to delineate forest cover and basal area after mixed-severity fires. Sustainability 10, 2227.

Sankey, T.T., McVay, J., Swetnam, T.L., McClaran, M.P., Heilman, P., Nichols, M, 2018. UAV hyperspectral and LiDAR data and their fusion for arid and semi-arid land vegetation monitoring. Remote Sensing Ecology Conservation 4, 20–33.

Sanz-Ablanedo, E., Chandler, J.H., Rodríguez-Pérez, J.R., Ordóñez, C., 2018. Accuracy of unmanned aerial vehicle (UAV) and SfM photogrammetry survey as a function of the number and location of ground control points used. Remote Sensing 10, 1606.

Schlesinger, W.H., Ward, T.J., Anderson, J, 2000. Nutrient losses in runoff from grassland and shrubland habitats in southern New Mexico: II. field plots. Biogeochemistry 49, 69–86.

Shackelford, N., Renton, M., Perring, M.P., Hobbs, R.J, 2013. Modeling disturbance-based native invasive species control and its implications for management. Ecological Applications 23, 1331–1344.

Shao, G., Tang, L., Liao, J., 2019. Overselling overall map accuracy misinforms about research reliability. Landscape Ecology 34, 2487–2492.

Story, M., Congalton, R, 1986. Accuracy assessment: a user's perspective. Photogrammetric Engineering and Remote Sensing 52, 397–399.

Teleki, B., Sonkoly, J., Erdős, L., Tóthmérész, B., Prommer, M., Török, P., 2019. High resistance of plant biodiversity to moderate native woody encroachment in loess steppe grassland fragments. Applied Vegetation Science 23, 175–184.

Torres-Sánchez, J., López-Granados, F., Serrano, N., Arquero, O., Peña, J.M., 2015. High-throughput 3-D monitoring of agricultural-tree plantations with unmanned aerial vehicle (UAV) technology. PLOS ONE 10, e0130479.

US Climate Data. 2020a. Climate Hebbronville-Texas. Available at: https://www.usclimatedata.com/climate/hebbronville/texas/united-states/ustx0589. Accessed 11 December, 2020.

US Climate Data. 2020b. Climate Granbury-Texas. Available at: https://www.usclimatedata.com/climate/granbury/texas/united-states/ustx1920. Accessed 18 March, 2020.

US Climate Data. 2020c. Climate Kingsville-Texas. Available online: https://www.usclimatedata.com/climate/kingsville/texas/united-states/ustx0697. Accessed 02 June, 2020.

Wallace, L., Lucieer, A., Malenovský, Z., Turner, D., Vopěnka, P., 2016. Assessment of forest structure using two UAV techniques: a comparison of airborne laser scanning and structure from motion (SfM) point clouds. Forests 7, 62.

Walther, C.H., 2019.]. Response of tanglehead *(Heteropogon contortus)* to prescribed burning and cattle grazing [thesis. Texas A&M University–Kingsville, Kingsville, TX, USA, p. 93 Available at.

Wang, D., Xin, X., Shao, Q., Brolly, M., Zhu, Z., Chen, J, 2017. Modeling aboveground biomass in Hulunber grassland ecosystem by using unmanned aerial vehicle discrete LiDAR. Sensors 17, 1–19.

Web Soil Survey. 2020a. AOI of study site Jim Hogg County. Available at: https://websoilsurvey.sc.egov.usda.gov/App/WebSoilSurvey.aspx. Accessed 11 December, 2020.

Web Soil Survey, 2020b. AOI of study site Hood County. Available at: https://websoilsurvey.sc.egov.usda.gov/App/WebSoilSurvey.aspx. Accessed 18 March, 2020.

Web Soil Survey. 2020c. AOI of study site Kleberg County vailable at: https://websoilsurvey.sc.egov.usda.gov/App/WebSoilSurvey.aspx. Accessed 03 June, 2020.

Wilcox, B.P., 2007. Does rangeland degradation have implications for global streamflow? Hydrology Process 21, 2961–2964.

Yilmaz, M.T., Hunt, E.R., Goins, L.D., Ustin, S.L., Vanderbilt, V.C., Jackson, T.J, 2008. Vegetation water content during SMEX04 from ground data and Landsat 5 Thematic Mapper imagery. Remote Sensing Environment 112, 350–362.

Zainuddin, K., Jaffri, M.H., Zainal, M.Z., Ghazali, N., Samad, A.M., 2016. Verification test on ability to use low-cost UAV for quantifying tree height. IEEE International Colloquium on Signal Processing & Its Applications (CSPA) 12, 317-321. Accessed 10 January 2021.

Zarco-Tejada, P.J., Diaz-Varela, R., Angileri, V., Loudjani, P., 2014. Tree height quantification using very high-resolution imagery acquired from an unmanned aerial vehicle (UAV) and automatic 3D photo-reconstruction methods. European Journal of Agronomy 55, 89–99.

Zhang, H., Sum, Y., Chang, L., Qin, Y., Du, J., Yi, S., Wang, Y, 2018. Estimation of grassland canopy height and aboveground biomass at the quadrant scale using unmanned aerial vehicle. Journal of Remote Sensing 10, 851.